Band-specific phase engineering for curving and focusing light in waveguide arrays

Ioannis D. Chremmos* and Nikolaos K. Efremidis
Department of Applied Mathematics, University of Crete, 71409 Heraklion, Greece
(Received 21 May 2012; published 25 June 2012)

Band-specific design of curved light caustics and focusing in optical waveguide arrays is introduced. Going beyond the discrete, tight-binding model, which we examined recently, we show how the exact band structure and the associated diffraction relations of a periodic waveguide lattice can be exploited to phase-engineer caustics with predetermined convex trajectories or to achieve optimum aberration-free focal spots. We numerically demonstrate the formation of convex caustics involving the excitation of Floquet-Bloch modes within the first or the second band and even multiband caustics created by the simultaneous excitation of more than one band. Interference of caustics in abruptly autofocusing or collision scenarios are also examined. The experimental implementation of these ideas should be straightforward since the required input conditions involve phase-only modulation of otherwise simple optical wavefronts. By direct extension to more complex periodic lattices, possibilities open up for band-specific curving and focusing of light inside two-dimensional or even three-dimensional photonic crystals.

DOI: 10.1103/PhysRevA.85.063830 PACS number(s): 42.25.Fx, 42.82.Et

I. INTRODUCTION

Waveguide arrays (WGAs) are a special kind of periodic optical media that have been attracting vivid research interest for quite some time [1,2]. In these photonic lattices, light propagates along the waveguides and at the same time it is dispersed across them through the evanescent interwaveguide coupling. This simple physical mechanism, called *discrete diffraction*, has profound implications on the macroscopic behavior of a WGA as an optical medium, enabling a diversity of linear and nonlinear phenomena that are absent in continuous media. Among them are discrete solitons [3,4], Bloch-momentum-dependent diffraction [5], Bloch oscillations [6] and surface Bloch oscillations [7,8], Rabi oscillations [9], Zener tunneling [10], perfect or fractional revivals [11], discrete Talbot effect [12], and dynamic localization [13]. The peculiar behavior of light inside waveguide lattices is owed to the photonic band structure that is associated with the periodic effective-index "potential." Each allowed band is characterized by a certain diffraction relation between the longitudinal (β) and the transverse (K) wave-vector component or Bloch momentum (BM), which accounts for the unusual beam dynamics in the lattice. For example, in a uniform medium, a light beam refracts monotonically with its input tilt. By contrast, the slope or *group velocity* (GV) ($v_g = -d\beta/dK$) of a discrete beam in a WGA attains a maximum value inside each allowed band and becomes zero at the band edges. Moreover, inside each allowed band, the diffraction coefficient ($D = d^2\beta/dK^2$) can be normal, anomalous, or zero depending on K, with the magnitude of diffraction increasing toward the band edges [5].

Although being essential for a number of exciting discrete diffraction phenomena, the band structure and the associated "anomalous" refractive behavior of light in WGAs preclude or complicate phenomena that are straightforward to obtain in continuous media. For example, and in contrast to the continuous case of Airy beams [14–16] there seem to be no diffraction-free solutions propagating in one-dimensional (1D) WGAs, other than the Floquet-Bloch (FB) modes, i.e., the physical modes of the periodic system. Also, since GV does not vary monotonically with the transverse wave number, it is not so straightforward to design beams with curved trajectories in WGAs, as it is in continuous media, where optical caustics with arbitrary convex trajectories can be obtained by an appropriate phase modulation of the input wavefront [17,18].

Nonetheless, there has recently been some interest in the design of beams that can follow curved trajectories inside WGAs. In [19], Wannier-Stark states were shown to write hyperbolic curves in uniform waveguide lattices that can be described by the tight-binding model. In the limit of slowly varying fields across the lattice, the connection of Wannier-Stark states with continuous Airy beams was also established. In a more general approach, we have recently investigated the design of arbitrary optical caustics in periodic waveguide lattices [20]. Specifically, we showed how different families of caustics, of the fold and cusp catastrophe type, result from discrete input beams that are phase modulated with a power law. Taking into account the sinusoidal dispersion relation [$\beta = 2\kappa\cos(K\Lambda)$ κ being the coupling coefficient between adjacent waveguides and Λ the lattice constant] that follows from the tight-binding model, we also determined the phase modulation required to create arbitrary power-law caustics or to achieve aberration-free focusing.

Discrete (tight-binding) models, such as that adopted in [20], can account only for propagation within the first allowed band. In this context, only half of the first Brillouin zone ($|K| \leqslant \pi/2$) can be used to create caustics, i.e., the part corresponding to rays whose slope increases with increasing K. The maximum slope of the participating rays within this band is 2κ. This in turn limits the slope of the trajectories that can be designed. However, GV can be increased if higher bands are excited. Therefore, if one is able to determine the dispersion features of higher bands, there will be significant additional freedom in designing curved trajectories.

In the present work we examine the design of optical caustics inside WGAs beyond the limits of the tight-binding (or coupled-mode) model. Specifically, we adopt a paraxial model of light propagation in a continuous sinusoidal potential,

*jochremm@central.ntua.gr

that is both simple and realistic. Such a model accounts for the continuous evolution of the optical field across a periodic lattice and thus for propagation in higher bands that are neglected by discrete models. The full band structure of the lattice can be determined numerically by Fourier-series expanding the FB modes and by solving the resulting eigenvalue problem, a method that is familiar in solid-state physics [21] and photonic crystals [22].

Having determined the band structure of the WGA, it is straightforward to derive GV as a function of the BM from the corresponding dispersion relation within each allowed band. This can subsequently be used to determine the input phase modulation that will produce a desired caustic, which is the essence of our *band-specific* engineering approach. The equation relating the input phase with the ray trajectory is similar to that in a continuous medium and follows from a stationary phase approximation to the integral transform of the optical field inside the WGA. In discrete approaches, e.g., [5] or [20], this integral is obtained with a discrete Fourier transform of the input condition. In the continuous case, one must take into account that the input field is decomposed into FB modes.

Ideally, to excite a desired band with BM K, the input optical field in a WGA should conform to the profile $\psi_K(x)$ of the corresponding FB mode. To create curved caustics however, K must vary continuously across the input plane ($z = 0$), so that the slope of the emitted rays follows the shape of the caustic. Thus an optimum input field would be a continuously varying FB profile $\psi_{K(x)}(x)$, which is, however, very specific and difficult to realize. Fortunately, in practice, propagation in higher bands (beyond the third) is very similar to propagation in free space and the corresponding FB modes are very much like plane waves, which is particularly true for weakly modulated lattices. This allows higher bands to be excited quite effectively with a phase-only modulation of a simple optical envelope (e.g., Gaussian or exponential). Moreover, as our simulations show, for weakly modulated lattices, even the lower bands can be excited fairly well with a phase-only modulation. In this empty-lattice-like approximation, a given input modulation $\exp(iKx)$ excites efficiently only the corresponding FB mode of band with number $\lceil K/\pi \rceil$. For continuously varying BM along x, the phase modulation should be $\exp[i\int_0^x K(\xi)d\xi]$, so that the neighborhood of x is occupied by a wave packet with local wave number $K(x)$. The above should be contrasted to the discrete approach, where one is limited to the first band and the critical parameter is the modulo-2π phase difference between adjacent waveguides.

It should be mentioned that a different, "side-coupling" method was proposed in [23] in order to selectively excite a single FB mode with a given longitudinal wave number β, which can be useful in strongly modulated lattices. For the purpose of the present work, however, we will adopt the simpler head-on excitation.

In the next sections we demonstrate band-specific engineering of caustics in a WGA. Excitation of the first band is suggested when the rays involved in the formation of a caustic or a single focus do not bend more than the maximum allowed GV in that band. For larger ray inclinations, the nth ($n = 2,3,...$) band can be used and the resulting BM satisfies $K(x) \geqslant (n-1)\pi$. It is also possible to create hybrid, multiband caustics that span more than one band. For example, the first part of the caustic may be formed by rays within the first band and the second part by rays within the second band. In the transition point, $K(x)$ must have a discontinuity such that the caustic continues with the same slope. We also show how all rays of an optical wavefront can be made to intersect at a single point inside the WGA and produce an aberration-free focal spot of high quality.

II. BAND-SPECIFIC ENGINEERING OF CAUSTICS AND FOCUSING

Consider the following continuous model for light propagation in a WGA:

$$iu_z + \tfrac{1}{2}u_{xx} + V(x)u = 0, \tag{1}$$

where spatial coordinates are normalized and the lattice of waveguides is described by the simple periodic potential $V(x) = V_0\cos(2\pi x)$. The period of the lattice has been set equal to unity. To determine the band structure of this array we expand an arbitrary FB mode in a Fourier series

$$\psi_K(x,z) = e^{i(Kx+\beta z)}\Psi_K(x) = e^{i(Kx+\beta z)}\sum_{n=-\infty}^{+\infty} c_{n,K}e^{i2\pi nx}, \tag{2}$$

where K is the BM, β is the propagation constant, and the series factor $\Psi_K(x)$ is the envelope of the FB mode conforming to the periodicity of the lattice. Substituting Eq. (2) into Eq. (1) and using the orthogonality of the Fourier harmonics, we end up with the linear system

$$-\tfrac{1}{2}(K+2n\pi)^2 c_{n,K} + \sum_{m=-\infty}^{+\infty} v_{n-m}c_{m,K} = \beta c_{n,K}, \tag{3}$$

where v_n are the Fourier series coefficients of $V(x)$. By truncating the infinite system, β follows as an eigenvalue of the matrix denoted by the left-hand side of Eq. (3). Ordering the eigenvalues in descending order, for each K, we obtain the complete band structure of the WGA, with the largest eigenvalue corresponding to the first band and so on. The corresponding eigenvectors can be substituted into Eq. (2) to return the FB wave functions. In the present case of a sinusoidal potential, $v_1 = v_{-1} = V_0/2$ are the only nonzero coefficients, hence the system matrix is tridiagonal Toeplitz.

Figure 1(a) shows the computed band structure in the case of $V_0 = 5$. A reduced zone scheme is used showing only the positive part of the first Brillouin zone. Differentiating the dispersion relation of each band, the GV is derived and shown in Fig. 1(b). For visualization purposes, an extended zone scheme is now used, according to which the nth band occupies the BM interval $(n-1)\pi \leqslant K \leqslant n\pi$. Within each band, the GV assumes a maximum value, while being zero at the edges where Bragg reflection occurs. The maximum value increases with increasing band number. Also, already from the third band, v_g starts to vary almost linearly with K having sharp zeros at the band edges. This is because, with increasing BM, propagation in the WGA becomes much like propagation in an unmodulated, continuous medium ($V_0 = 0$), FB modes resemble plane waves, and the dispersion relation,

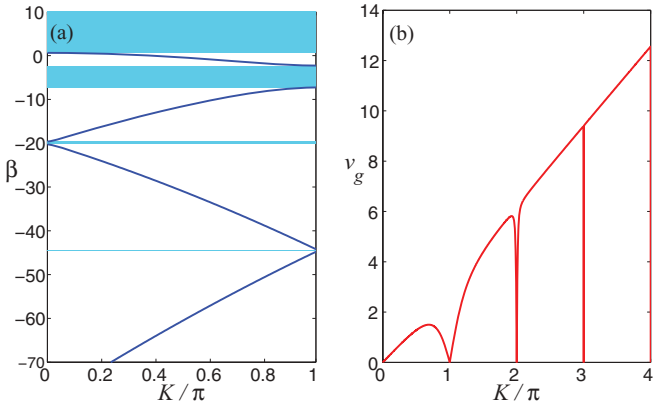

FIG. 1. (Color online) (a) Band structure and (b) GV ($v_g = -d\beta/dK$) versus BM for a WGA described by the potential $V(x) = 5\cos(2\pi x)$.

within the paraxial approximation, becomes almost parabolic ($\beta \approx -K^2/2$).

Consider now an arbitrary optical beam $u_0(x)$ launched into the WGA. By the completeness of the FB eigenfunctions, the input condition can be expressed as the continuous superposition

$$u_0(x) = \int_{-\infty}^{+\infty} C(K)\Psi_K(x)e^{iKx}\,dK. \tag{4}$$

An extended scheme has again been used for the BM, according to which the FB mode Ψ_K belongs to the band with number $\lceil |K|/\pi \rceil$. The weight function follows easily by the orthogonality of the FB modes

$$C(K) = \int_{-\infty}^{+\infty} u_0(\xi)\Psi_K^*(\xi)e^{-iK\xi}\,d\xi. \tag{5}$$

Now, since each FB mode in the expansion of Eq. (4) propagates with its own constant $\beta(K)$, it is straightforward to combine the last two equations to write the optical field anywhere inside the WGA as the double integral

$$u(x,z) = \int_{-\infty}^{+\infty}\int_{-\infty}^{+\infty} u_0(\xi)\Psi_K(x)\Psi_K^*(\xi)e^{i[K(x-\xi)+\beta z]}\,dK\,d\xi. \tag{6}$$

In designing caustics and focusing, the input field can be expressed as a phase-modulated envelope, i.e., $u_0(\xi) = A(\xi)\exp[i\phi(\xi)]$. Substituting into Eq. (6), the total phase in the exponential becomes $Q = \phi(\xi) + K(x-\xi) + \beta z$. In a stationary-phase approximation to the above integral, the conditions are posed $Q_\xi = Q_K = 0$, from which we obtain

$$x = \xi + v_g(K)z, \tag{7}$$

where $K = \phi'(\xi)$. Equation (7) is essentially the equation of a ray starting from the x axis point $x = \xi$ and traveling at a slope $v_g(\xi) = -\beta'(K(\xi))$, with the local BM being determined by the derivative of the input phase. Note that the slope $v_g(\xi)$ of the ray is essentially a local form of GV assigned to the wave packet around position ξ, and should not be confused with the GV of a wide (narrow-band) beam as a whole. Hence the modulated wavefront can be thought as a continuous train of wave packets each having its own GV. Also note that, in applying the stationary-phase method, the variation of the periodic envelopes Ψ_K of the FB modes with K in Eq. (6) has been assumed to be slow, which is true for weakly modulated lattices. In any case, the success of the very useful but approximate ray picture must be evaluated in comparison to more rigorous wave simulations, as will be done in the next section.

For a given phase modulation, Eq. (7) can be used to parametrically determine the equation of the caustic, namely, the envelope of the bundle of rays emanating from all ξ. Differentiating Eq. (7) with respect to ξ and taking into account that the GV of a ray is equal to the slope of the caustic at the touching point ($v_g = dx/dz$), one obtains

$$(x,z) = \left(\xi - \frac{v_g(\xi)}{v_g'(\xi)}, -\frac{1}{v_g'(\xi)}\right), \tag{8}$$

where v_g is implied to be a function of ξ as $v_g(\xi) = -\beta'(\phi'(\xi))$. It also follows from the chain rule that $v_g'(\xi) = v_g'(K)\,K'(\xi)$. From the latter, the importance of the relation $v_g(K)$ between GV and BM in the formation of caustics in a WGA is clear. This remark is the key to band-specific engineering of caustics, in the sense that the input phase modulation depends critically on the excited band and its associated dispersion properties. By contrast, in a continuous medium, β is a quadratic function of K (within the paraxial regime), hence $v_g(K)$ is a linear function, $v_g'(K)$ is a constant, and the shape of the caustic is determined solely by the input phase $\phi(\xi)$.

In an inverse design approach one first specifies the function of the caustic $x = f(z)$. An arbitrary tangent ray to this curve has a slope $v_g = f'(z)$ and intersects the input plane at the point $\xi = f(z) - zf'(z)$. By inverting the last equation, z can be determined as a function of ξ. The dispersion properties of the periodic medium are expressed through a function $v_g = G(K)$, from which one readily obtains BM as a function of the input position as $K(\xi) = G^{-1}(v_g(\xi))$. Finally integrating $K(\xi) = \phi'(\xi)$, the required phase is given by

$$\phi(\xi) = \int_0^\xi K(\chi)\,d\chi = \int_0^\xi G^{-1}(v_g(\chi))d\chi, \tag{9}$$

where inside the integral ξ has been replaced by χ, the integration variable. Note that in a periodic medium, such as a WGA, function $G(K)$ is not one to one [Fig. 1(b)]. Therefore, in order that the inverse function G^{-1} is single valued, the BM is restricted to the part of a Brillouin zone where the GV is increasing. When more than one band participates in the formation of a caustic, G^{-1} experiences discontinuities, which, however, do not affect the integration in Eq. (9). For example, referring to Fig. 1(b), for $0 \leqslant v_g < 1.5$, G^{-1} returns BM values $0 \leqslant K < 0.69\pi$ within the first band, while for $1.5 \leqslant v_g < 5.8$, it returns values $1.1\pi \leqslant K < 1.93\pi$ within the second band. Therefore, at $v_g = 1.5$, the maximum GV within the first band, G^{-1}, experiences a discontinuity. The next discontinuity is at $v_g = 5.8$, the maximum GV within the second band, where the BM jumps to the third band and so on. For higher bands, the GV varies almost linearly with K and the discontinuities occur approximately at $v_g = n\pi$, i.e., very close to the Bragg resonances. In this regime the jumps of the BM are very small and have a little effect on the computation

of the input phase, which physically means that the periodic medium responds as a continuous one.

Let us now consider the case of focusing. To focus an optical beam, an appropriate phase modulation should be imparted to it so that the constituent rays converge to a single point. This implies that the GV (or slope) of any ray must be proportional to the distance of its starting point from the center of the beam. In a continuous medium and within the paraxial propagation regime, this is achieved with a parabolic phase $\phi(\xi) = -\xi^2/2f$, which is most conveniently imposed by passing the beam through a thin lens with focal distance f. Indeed, a parabolic phase induces a transverse wave number $K(\xi)$ that varies linearly with ξ. Since the dispersion equation of a continuous medium is also parabolic ($\beta = -K^2/2$), the GV of rays is proportional to K, and hence proportional to ξ. Therefore all rays meet at a single point. In a WGA, however, the dispersion relation $\beta(K)$ is not parabolic and a parabolic input phase results in a focus that suffers from spherical aberrations [20]. Due to the band structure, the GV satisfies $v_g(K) < K$, hence rays bend less than required (negative aberrations), creating a cusp catastrophe, i.e., two symmetric fold type caustics that originate at a zero angle from the intended focus.

To achieve aberration-free focusing in a WGA, the GV should be made to vary linearly with distance from the center or $v_g = -\xi/z_f$, z_f being the distance to the desired focus inside the array. Note that the minus sign denotes that the rays bend inward. Then, according to the previous discussion, the Bloch wave number should vary with ξ as $K(\xi) = G^{-1}(-\xi/z_f)$, where G^{-1} is now assumed to extend to negative arguments as an odd function, i.e., $G^{-1}(-\xi) = -G^{-1}(\xi)$. The phase is finally determined by integrating $\phi'(\xi) = K(\xi)$ as in Eq. (9) and is an even function of ξ.

It is obvious that, for beams with a sufficient initial width and/or an appropriate focal distance, focusing may involve rays from more than one band. The jump of the local BM (function G^{-1}) to the next higher band occurs at $\pm\xi$ where the slope $|\xi|/z_f$ of the corresponding ray exceeds the maximum GV of the current band. It is also possible to excite only one band by accordingly restricting the values of function G^{-1}. For example, as we will show in the next section, if the maximum slope of the focusing rays is larger than the maximum GV of the first band but smaller than the maximum GV of the second band, one can arrange that G^{-1} returns values $K \geqslant \pi$, so that all rays stay within the second band. This is characteristic of the freedom in design offered by band-specific phase engineering.

It is also worth mentioning that the phase resulting from Eq. (9) depends on the construction of function G^{-1} and is not unique. One may construct this function in infinite ways by choosing the discontinuity points to be at GV values lower than the maxima of each band. However, we have here opted to utilize each band up to its maximum GV.

III. NUMERICAL EXAMPLES

In this section we demonstrate band-specific engineering of caustics and aberration-free focusing inside a WGA through several numerical examples. In all cases, the input condition $u_0(\xi)$ has been propagated in the WGA by solving Eq. (1) with a fourth-order Runge-Kutta scheme. In all of the examples, the amplitude of the sinusoidal lattice potential has been assumed $V_0 = 5$.

Power laws are a familiar model for convex optical caustics. Assuming the general function $f(z) = \gamma z^\delta$, where $\gamma > 0$ and $\delta > 1$, and following the discussion of Sec. II, it is easy to show that this caustic is constructed by rays starting from points ξ on the negative x axis and that their GV is given as a function of ξ by

$$v_g(\xi) = v_{g0}\left(\frac{\xi}{\xi_0}\right)^{(\delta-1)/\delta}, \tag{10}$$

where v_{g0} is the GV of the ray starting from point $\xi_0 < 0$ on the input plane. If the input wavefront (or practically most of its power) is confined from ξ_0 to 0, then v_{g0} is the maximum GV and determines the bands that must be excited to create this caustic. Using Eqs. (8) and (10), it can also be shown that this extreme ray touches the caustic at the point (x_0, z_0), where $x_0 = \xi_0/(1-\delta)$ and $z_0 = \delta\xi_0/v_{g0}(1-\delta)$. In the following we use ξ_0, v_{g0}, and δ to parametrically define the caustics to be designed.

A. First band caustics

Figure 2 shows two examples of caustics in a WGA that are designed by exciting rays mainly within the first allowed band. In both cases, the input wavefront is confined to negative values of ξ using the simple envelope $A(\xi) = (e^{-0.1\xi} + e^{5\xi})^{-1}$, which decays slowly as $e^{0.1\xi}$ for decreasing negative ξ and strongly as $e^{-5\xi}$ for increasing positive ξ. The phase of the beam is provided by Eq. (9). At point $\xi_0 = -20$, where the input amplitude has dropped to 0.15 of its maximum value, the group velocity v_{g0} is lower or equal than the maximum GV within the first band. Note how the optical field propagates in the form of a curved beam, staying confined around integer values of x, namely, within the maxima of the potential $V(x)$—the waveguides—which is indicative of the characteristic profile of the FB modes within the first band. The success of the design is verified by the superposed curves $x = \gamma z^\delta$, which agree very well with the simulated trajectories of the beams. It is remarkable that these curved trajectories are achieved by phase modulating an otherwise simple optical wavefront, suggesting

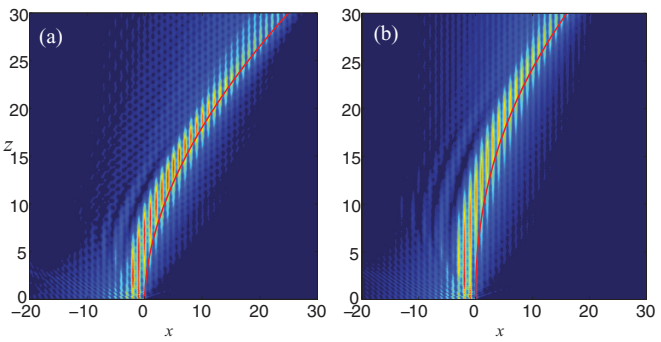

FIG. 2. (Color online) Caustics in a WGA under excitation of the first band. The design parameters are (a) $\delta = 1.8$, $\xi_0 = -20$, $v_{g0} = 1.5$ and (b) $\delta = 2.2$, $\xi_0 = -20$, $v_{g0} = 1.2$. The equations of the caustics are $f(z) = 0.055z^{1.8}$ and $f(z) = 0.009z^{2.2}$, respectively, and are superposed as red curves. In both cases, the envelope of the input beam is $A(\xi) = (e^{-0.1\xi} + e^{5\xi})^{-1}$.

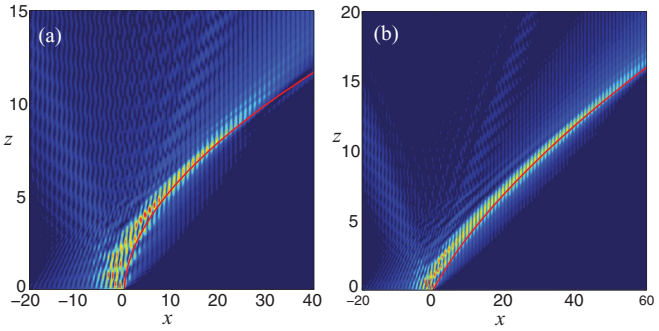

FIG. 3. (Color online) Caustics in a WGA under excitation of the second band. The design parameters are (a) $\delta = 1.8$, $v_{g0} = 5$, $\xi_0 = -20$, $\alpha = 0$ and (b) $\delta = 1.8$, $v_{g0} = 5$, $\xi_0 = -20$, $\alpha = 2$. The corresponding equations are $f(z) = 0.4790z^{1.8}$ and $f(z) = 2z + 0.1910z^{1.8}$, respectively, and are superposed as red curves. The envelope of the input beam and the lattice potential are the same as Fig. 2.

that the experimental implementation of these caustics should be straightforward by reflecting the beam on a spatial light modulator (SLM) programed with phase $\phi(\xi)$, just before it enters the front facet of the WGA.

B. Second band caustics

Caustics with higher slopes can be designed by exciting rays within the second band. This is achieved by letting function G^{-1} return BM values $K \geqslant \pi$ in Eq. (9). For example, Fig. 3(a) shows the case of a caustic with order $\delta = 1.8$, which reaches a GV $v_{g0} = 5$ at the contact point with the ray that is emitted from input point $\xi_0 = -20$. The input envelope is the same as that of Fig. 2(a). The result of the simulation shows that, although the expected caustic is reproduced fairly well, the field initially experiences oscillations that were not present in the case of Fig. 2. These oscillations are a result of interference between FB modes located at the $K = \pi$ edge of the first and the second bands, which are simultaneously excited near the input plane. To see why this is happening, note that, in order to excite the second band, we have let the BM assume values $K \geqslant \pi$. This implies that, for a caustic with zero initial GV and close to $\xi = 0$, the input wave locally resembles $\exp(i\pi\xi) = \cos(\pi\xi) + i\ \sin(\pi\xi)$. The real part of this wave function corresponds to a wave that has maximum energy within the high-index regions and an alternating sign. This clearly excites the FB mode located at the $K = \pi$ (low) edge of the first band. The imaginary part, on the other hand, is a wave that also has an alternating sign but which is maximum *in between* the waveguides having field nodes inside them. This condition clearly excites the FB mode located at the $K = \pi$ (high) edge of the second band. The local interference of the two modes is responsible for the observed distorted, oscillating image of the field close to the input plane. At longer propagation distances, the oscillations fade out and the beam propagates along a curved path staying confined to the low-index regions, indicating the pure excitation of the FB modes of the second band. Figure 3(b) shows another example of a caustic created using the second band, however with a nonzero initial GV. Such a caustic is expressed by the curve $f(z) = \alpha z + \gamma z^{\delta}$, where $v_g(0) = \alpha$ is the initial GV (or tilt).

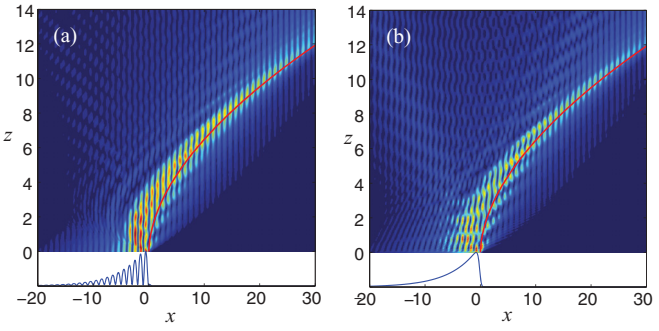

FIG. 4. (Color online) Caustics in a WGA under excitation of the second band. The input beam amplitude $A(\xi)$ is a continuous FB mode envelope in (a) and $A(x) = (e^{-0.1x} + e^{5x})^{-1}$ in (b). The input phase is the same in both cases and results from Eq. (9), where GV is given by Eq. (10) with the parameters $\delta = 1.8$, $\xi_0 = -30$, and $v_{g0} = 5$. The bottom blue curves are the intensity of the input beam, while the superposed red curves are the caustic $x = 0.346z^{1.8}$.

In this case, Eq. (10) is modified to

$$v_g(\xi) = \alpha + (v_{g0} - \alpha)\left(\frac{\xi}{\xi_0}\right)^{(\delta-1)/\delta}. \tag{11}$$

Now the extreme ray, starting from ξ_0 with slope v_{g0}, touches the caustic at the point (x_0, z_0), where $z_0 = \delta\xi_0/(v_{g0} - \alpha)(1 - \delta)$ and $x_0 = \alpha z_0 + \xi_0/(1 - \delta)$. As shown by the simulation, this caustic has a clearer intensity profile with weaker initial distortion. This should be expected by the fact that, due to the initial tilt, the input BM starts from a value $K > \pi$, thus mainly exciting FB modes of the second band.

The initial distortion of the beam observed in Fig. 3(a) can be reduced if the WGA is optimally excited with a beam whose amplitude is a continuous varying, according to the input BM, FB envelope. Specifically, if $K(\xi) = G^{-1}(v_g(\xi))$ is the input BM required to create a given caustic, the amplitude of the input beam is taken to be $A(\xi) = \Psi_{K(\xi)}(\xi)$, where Ψ_K is the periodic envelope of the FB mode with BM K, as defined below Eq. (2). The resulting envelope is subsequently modulated by the phase obtained from Eq. (9) as in the previous examples. To better illustrate the improvement achieved with such a particularly designed input condition, we have let the

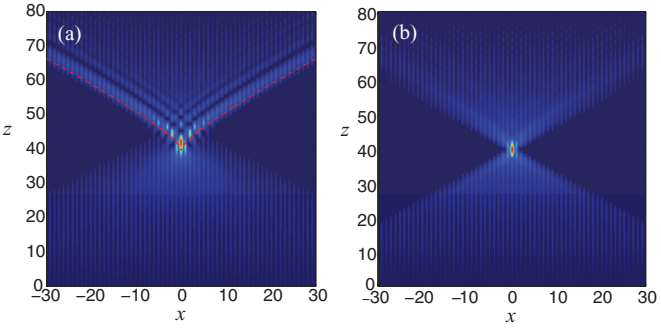

FIG. 5. (Color online) Focusing in a WGA using (a) the parabolic phase $\phi(\xi) = -\xi^2/70.4$ imposed on the envelope $A(\xi) = \exp[-(\xi/76)^{20}]$ and (b) the phase resulting from Eq. (9) with $v_g(\xi) = -\xi/40$, imposed on the envelope $A(\xi) = \exp-(\xi/60)^{20}]$. The dashed red curves in (a) are the twin fold type caustics that create the cusp.

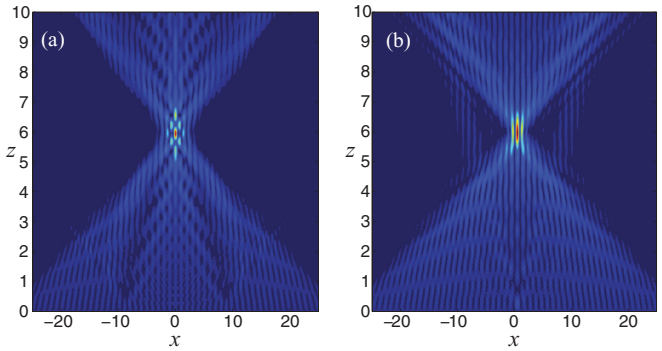

FIG. 6. (Color online) Focusing in a WGA using the phase resulting from Eq. (9) with (a) $v_g(\xi) = -\xi/6$ and (b) $v_g(\xi) = -(\xi - 0.5)/6$, imposed on the envelope $A(\xi) = \exp\left[-(\xi/30)^{20}\right]$. The input BM assumes values $K \geqslant 0$ in (a), hence exciting the first and second bands, and $K \geqslant \pi$ in (b) hence exciting only the second band.

BM assume values $K \geqslant \pi$ in order to excite the second band. The result of the simulation is shown in Fig. 4(a), in comparison to the case of a simple exponential envelope shown in Fig. 4(b). As expected, in the first case, the specifically engineered input amplitude facilitates the pure excitation of the FB modes of the second band, hence the initial evolution of the beam is smoother. By contrast, the second case suffers from intensity oscillations, the result of the simultaneous excitation of the $K = \pi$ edges of the first and second bands. However, it should be noted that the improved behavior of Fig. 4(a) is at the cost of a more difficult to realize input wavefront.

C. Focusing

Let us now examine the case of focusing. As mentioned, using a parabolic phase to focus a beam inside a WGA leads to a focus that suffers from negative spherical aberrations. Such a phase is given by $\phi(\xi) = -\xi^2/2f$, where f is the focal distance of a lens that induces the same phase to a transmitted wavefront. Since GV is generally smaller inside the WGA than in the unmodulated lattice ($V_0 = 0$), f is smaller than the actual distance z_f at which the focus will be created in the WGA. Specifically, using Eq. (8), it can be shown that $f = D_0 z_f$,

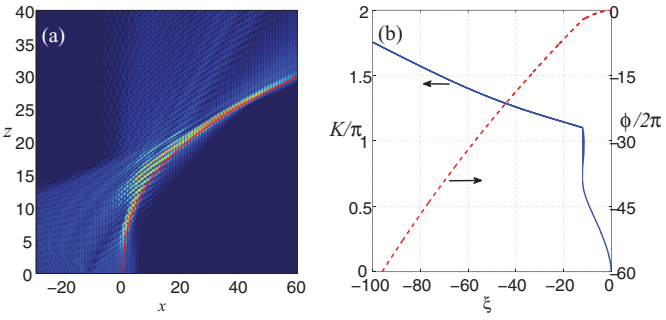

FIG. 7. (Color online) (a) Caustic in a WGA under the excitation of two bands. The parameters for the phase engineering are $\delta = 2.5$, $v_{g0} = 1.5$, and $\xi_0 = -12$. (b) BM (solid, blue line, left ordinate) and phase (dashed, red line, right ordinate) of the input beam. The amplitude of the input beam is $A(\xi) = \exp[-(\frac{x+45}{50})^{30}]$.

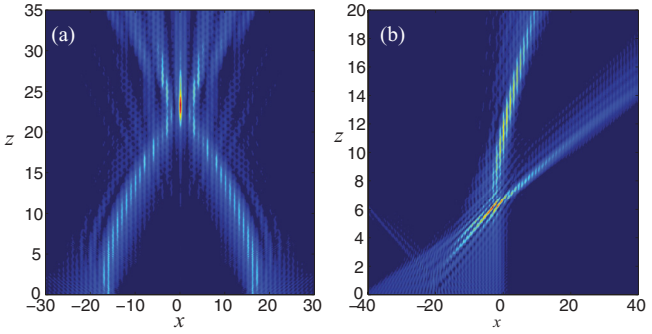

FIG. 8. (Color online) (a) Interference of two symmetric, opposite accelerating caustics. The parameters of the caustics are the same as Fig. 2(a). (b) Collision of caustics from the first and second bands excited simultaneously by the same input wavefront. The input BM varies linearly with slope $0.688\pi/20$ and a 0.5π jump to the second band at $\xi = -20$. The amplitude of the input beam in (b) is $A(\xi) = \exp[-(\frac{x+21}{22})^{20}]$.

where $D_0 = \left(dv_g/dK\right)_{K=0}$ is the diffraction coefficient at the top edge of the first band. To determine the maximum width $2\xi_0$ of the wavefront that can be focused, one requires that the extreme rays starting from $\pm\xi_0$ have the maximum GV within the first band, i.e., $\xi_0 = fK_{\max}$, where $K_{\max}$ is the BM where the maximum GV occurs. These two rays are the asymptotes of the twofold-type caustics that bifurcate from point $z = z_f$ to create the cusp catastrophe. An example is shown in Fig. 5(a), where the focal distance inside the WGA is set to $z_f = 40$. For our lattice with $V_0 = 5$, $D_0 \approx 0.88$ and $K_{\max} \approx 0.688\pi$. The result clearly verifies the formation of the cusp as indicated by the evident curved intensity wings that develop outward beyond the focus.

The aberrations can be eliminated with band-specific phase engineering. Using the phase given by Eq. (9) with $v_g(\xi) = -\xi/z_f$ implies that all rays are forced to pass from the on-axis point $z = z_f$, and thus create an optimum focus. The maximum beam width is again determined by the extreme rays as $\xi_0 = z_f v_{g,\max}$, where $v_{g,\max} = G(K_{\max})$ is the maximum GV within the first band. The result of the corresponding simulation is shown in Fig. 5(b) and is very satisfactory. The aberrations have been completely eliminated and the quality of the focus has been significantly improved. Note that in both examples of Fig. 5 a super-Gaussian envelope has been assumed.

We now consider a case of focusing involving larger values of GV. An example is shown in Fig. 6(a), where a super-Gaussian wavefront with width 60 is focused at a distance $z_f = 6$. The input phase is obtained from Eq. (9) with $v_g(\xi) = -\xi/z_f$. For $|\xi| \leqslant 9$, we have $v_g(\xi) \leqslant v_{g,\max}$ and the BM resulting from function G^{-1} is within $0 \leqslant K \leqslant K_{\max}$, hence the first band is excited. For larger $|\xi|$, the BM jumps into the interval $\pi < K < 2\pi$ and the second band is excited. The excitation of the two bands is evident in the simulation if one carefully observes the confinement of the field in the high- and low-index regions. Note how all rays focus at the desired point, which is, however, surrounded by secondary intensity maxima, in contrast to the clear focus of Fig. 5(b). This is obviously the result of interference between the different envelopes of the FB modes of the first and second bands in the neighborhood of the focus. Focusing using only the second band is demonstrated

in Fig. 6(b). As mentioned, excitation of the second band is achieved by letting function G^{-1} obtain values $K \geqslant \pi$ for all positive values of GV. Attention should be paid to the fact that, since FB modes of the second band have field nodes inside the high-index regions, effective focusing can be achieved only in the low-index regions. For this reason, the GV in this case is chosen as $v_g(\xi) = -(\xi - 0.5)/6$ so that all rays intersect at the *off-axis* point $(0.5, z_f)$. The result verifies the expected behavior. At the desired focal distance, power is indeed confined in the potential valley around $x = 0.5$, although with some secondary power maxima in the adjacent lattice periods.

D. Caustics interference

Two or more bands can be simultaneously excited and cooperate to create a given caustic. For example, rays of the first band can create the initial part of the caustic, in which the GV stays lower than $v_{g,\max}$, and then the second band takes over to account for the part with larger slopes. A characteristic example is shown in Fig. 7(a) for the caustic $x = 0.012z^{2.5}$. In this case, rays emanating from the interval $-12 \leqslant \xi \leqslant 0$ have GV in the range $0 \leqslant v_g \leqslant 1.5$ and BM within the first band [Fig. 1(b)]. At around $\xi = -12$ the BM has a discontinuity jump to the point with equal GV within the second band and the caustic continues smoothly. The input phase $\phi(\xi)$ is determined by integrating this function and is a continuous function with a discontinuous derivative at $\xi = -12$. Both BM and phase versus ξ are shown in Fig. 7(b). The numerical simulation of Fig. 7(a) verifies the expected behavior. In the initial part of the caustic the field is confined—-although with some oscillations—in the high-index regions manifesting the excitation of the FB modes of the first band. A region of interference between two bands follows and, after a certain point, the caustic is clearly constructed by rays of the second band, as the field confinement in the low-index region indicates. The shape of the caustic is verified by the superposed analytic curve.

Optical caustics can interact in many other ways. In continuous media, a remarkable case is that of abrupt autofocusing where a circular beam with Airy radial amplitude profile writes a parabolic caustic surface of revolution that collapses on axis on a point of large intensity gradient [24]. For 1D beams inside a WGA, an analogous phenomenon can be obtained when two mirror-symmetric, fold-type caustics, such as those of Fig. 2 or Fig. 3, are made to intersect. An example is shown in Fig. 8(a) using the caustic of Fig. 2(a). The obtained effect is very similar to autofocusing beams in free space. It is remarkable how power is confined at the focus within the central waveguide. Note, however, that the intensity contrasts obtained with 1D beams are much lower compared to two-dimensional (2D) beams because, in the latter case, the focus is formed by the interference of a continuum of rays emanating from a circle on the input plane. Another case of interfering caustics is shown in Fig. 8(b) where a linear input BM excites simultaneously the first two bands creating two colliding caustics. A notable interference effect is evident at the collision region where the low GV caustic of the first band, which is confined in the high-index regions, intersects the high GV caustic of the second band, which is confined in the low-index regions.

IV. CONCLUSION

We have investigated band-specific phase engineering of optical caustics and focusing inside WGAs. Taking into account the band structure and the associated dispersion equations of each allowed band, it is possible to determine the phase modulation that will force a simple optical wavefront to form a desired convex caustic. Caustics that involve the excitation of one or more bands are possible, with each band being assigned the part of the caustic whose slope is within the range of GV inside this band. The transitions between the bands are triggered by corresponding discontinuity jumps in the derivative of the input phase or the local BM. Band-specific phase engineering can also be used to create optimum focal spots inside a WGA, eliminating the spherical aberrations that occur when trying to focus a wavefront by means of a parabolic phase modulation. What we find particularly important is that such beams can be effectively designed in WGAs by a *phase-only* modulation of a simple optical wavefront, thus lending themselves to a straightforward experimental realization. Together with our recent work [20] on caustics in discrete optical lattices, the possibilities explored here expand the concept of curved light in general periodic optical structures. By properly exploiting the band structure and the resulting dispersion properties, it should also be possible to apply similar design procedures and observe analogous curved light phenomena inside 2D or even 3D photonic crystals.

ACKNOWLEDGMENT

This work was supported by the Archimedes Center for Modeling, Analysis and Computation (ACMAC) (project FP7-REGPOT-2009-1).

[1] D. N. Christodoulides, F. Lederer, and Y. Silberberg, Nature (London) **424**, 817 (2003).
[2] F. Lederer, G. I. Stegeman, D. N. Christodoulides, G. Assanto, M. Segev, and Y. Silberberg, Phys. Rep. **463**, 1 (2008).
[3] D. N. Christodoulides and R. I. Joseph, Opt. Lett. **13**, 794 (1988).
[4] H. S. Eisenberg, Y. Silberberg, R. Morandotti, A. R. Boyd, and J. S. Aitchison, Phys. Rev. Lett. **81**, 3383 (1998).
[5] T. Pertsch, T. Zentgraf, U. Peschel, A. Bräuer, and F. Lederer, Phys. Rev. Lett. **88**, 093901 (2002).
[6] U. Peschel, T. Pertsch, and F. Lederer, Opt. Lett. **23**, 1701 (1998).
[7] I. D. Chremmos and N. K. Efremidis, Opt. Lett. **37**, 1892 (2012).
[8] A. Perez-Leija, R. Keil, A. Szameit, A. F. Abouraddy, H. Moya-Cessa, and D. N. Christodoulides, Phys. Rev. A **85**, 013848 (2012).
[9] K. G. Makris, D. N. Christodoulides, O. Peleg, M. Segev, and D. Kip, Opt. Express **16**, 10309 (2008).

[10] H. Trompeter, T. Pertsch, F. Lederer, D. Michaelis, U. Streppel, A. Bräuer, and U. Peschel, Phys. Rev. Lett. **96**, 023901 (2006).
[11] N. K. Efremidis and D. N. Christodoulides, Opt. Commun. **246**, 345 (2005).
[12] R. Iwanow, D. A. May-Arrioja, D. N. Christodoulides, G. I. Stegeman, Y. Min, and W. Sohler, Phys. Rev. Lett. **95**, 053902 (2005).
[13] S. Longhi, M. Marangoni, M. Lobino, R. Ramponi, P. Laporta, E. Cianci, and V. Foglietti, Phys. Rev. Lett. **96**, 243901 (2006).
[14] G. A. Siviloglou and D. N. Christodoulides, Opt. Lett. **32**, 979 (2007).
[15] G. A. Siviloglou, J. Broky, A. Dogariu, and D. N. Christodoulides, Phys. Rev. Lett. **99**, 213901 (2007).
[16] Y. Hu, G. A. Siviloglou, P. Zhang, N. K. Efremidis, D. N. Christodoulides, and Z. Chen, in *Nonlinear Photonics and Novel Optical Phenomena*, edited by Z. Chen and R. Morandotti, Springer Series in Optical Sciences Vol. 170 (Springer, Berlin/Heidelberg, 2010).
[17] E. Greenfield, M. Segev, W. Walasik, and O. Raz, Phys. Rev. Lett. **106**, 213902 (2011).
[18] I. D. Chremmos, Z. Chen, D. N. Christodoulides, and N. K. Efremidis, Phys. Rev. A **85**, 023828 (2012).
[19] R. El-Ganainy, K. G. Makris, M. A. Miri, D. N. Christodoulides, and Z. Chen, Phys. Rev. A **84**, 023842 (2011).
[20] N. K. Efremidis and I. D. Chremmos, Opt. Lett. **37**, 1277 (2012).
[21] C. Kittel, *Introduction to Solid State Physics*, 6th ed. (Wiley, New York, 1986).
[22] J. D. Joannopoulos, S. G. Johnson, J. N. Winn, and R. D. Meade, *Photonic Crystals: Molding the Flow of Light*, 2nd ed. (Princeton University Press, Princeton, NJ, 2008).
[23] D. Mandelik, H. S. Eisenberg, Y. Silberberg, R. Morandotti, and J. S. Aitchison, Phys. Rev. Lett. **90**, 053902 (2003).
[24] N. K. Efremidis and D. N. Christodoulides, Opt. Lett. **35**, 4045 (2010).